SSRG International Journal of Mechanical Engineering
ISSN: 2348-8360/ https://doi.org/10.14445/23488360/IJME-V12I12P105

Volume 12 Issue 12, 45-53, December 2025

Original Article

Investigation of Microstructure and Mechanical Properties for API 51 X70 Steel Welded by Robotic Mig Welding

Nitin Gudadhe[1,2*], Mridul Singh Rajput[1], Sanjeev Kumar[1]

[1]*Department of Mechanical Engineering, National Institute of Technology, Raipur, Chhattisgarh, India.*
[2]*Department of Mechanical Engineering, Ramdeobaba University, Nagpur, Maharashtra, India.*

[*]*Corresponding Author : nitingudadhe94@gmail.com*

Received: 09 October 2025 Revised: 10 November 2025 Accepted: 12 December 2025 Published: 27 December 2025

Abstract *- In the present research, the investigation of the heat-affected zone behavior and weld metal characteristics in API 5L X70 pipeline steel welded using robotic Metal Inert Gas (Robo-MIG) process is studied. The microstructural evolution and its influence on mechanical properties are also analyzed for the same metal. Nine weld samples were fabricated using a Taguchi L9 orthogonal array experimental design. The input parameters, such as current (140-180 A), voltage (24-28 V), and welding speed (2.7-3.6 mm/s), varied systematically to perform various testing and characterization. This mechanical characterization consists of tensile testing, Vickers microhardness measurements, and Charpy V-notch impact testing at both room temperature and sub-zero conditions (-40°C to -100°C). Microstructural analysis is done using optical microscopy. This shows that the distinct phase transformations occur across the base metal, HAZ, and weld zone. It was observed that welding current exerts the most significant influence on mechanical properties. With an increase in the welding current from 140 A to 180 A, the hardness increases from 161 HV to 190 HV. The result shows that a current of 180 A, voltage of 26 V, and speed of 2.7 mm/s are the optimal input parameters, which yield output parameters as maximum tensile strength of 478 MPa and average hardness of 190 HV at a heat input of 2.9 kJ/mm. Due to the formation of Widmanstätten ferrite, bainite, martensite, and Martensite-Austenite (MA), the HAZ shows the highest hardness among all zones. Impact toughness evaluation revealed that the HAZ maintained adequate toughness (28 J average) at -40°C, meeting ASME requirements for cold-service applications. It is observed from the Microstructural analysis that lower heat input conditions produced finer grain structures with higher bainite content and pronounced acicular ferrite. This optimizes the strength-toughness balance. Higher heat input resulted in coarser grains with predominant Widmanstätten ferrite and elevated MA content. These findings reveal the detailed information for optimizing robotic MIG welding parameters to ensure structural integrity and reliable performance of API 5L X70 steel pipelines in oil and gas transmission applications.*

Keywords *- API 5L X70 steel, Robotic MIG welding, Microstructure, Impact toughness.*

1. Introduction

The growth in globalization and industrialization has significantly increased the demand for petroleum products. This generates the need for efficient oil and gas transportation systems. The advancement in transportation systems requires innovative technologies in pipeline manufacturing [1]. The pipelines are used in offshore environments subject to different environmental hazards. This may lead to their structural integrity and long-term serviceability, which includes soil erosion, ground corrosion, and slope instability. Due to this, the pipeline infrastructure may lead to substantial damage [2]. In addition to that, internal corrosion is also one of the critical challenges. It generates particularly when it meets transport corrosive agents such as hydrogen and seawater. It may affect the pipelines mostly in the welded areas. The performance of welded pipeline areas, such as joints, is mostly influenced by the welding systems [5]. This welded pipeline is mostly manufactured from steel. These structures are mostly exposed to sub-zero temperatures in Arctic pipelines and cryogenic storage tanks. However, at these low temperatures, these pipeline materials can undergo a ductile-to-brittle transition called DBT. This further increases the risk of a sudden fracture. The welded pipeline, particularly the HAZ, is subject to the weakest point because of microstructural changes and residual stresses. The Charpy V-Notch (CVN) is one of the impact tests widely used to evaluate the toughness of steels at low temperatures. Studies in literature have shown that the DBT temperature is strongly influenced by the microstructure of the materials, their chemical composition, and welding parameters. Lambert-

Perlade et al. [6] reported that weld metals that have high-toughness with acicular ferrite microstructure can exhibit superior low-temperature impact properties in comparison with those that have coarse bainitic or martensitic structures. Ding et al. [7] reported that the presence of inclusions and precipitates in the weld zone can act as stress concentrators, promoting crack initiation at cryogenic temperatures. During the welding process, residual stresses, microstructural heterogeneity, and potential defects were generated. They may further degrade the impact toughness of the materials. Kim et al. reported that Post-Weld Heat Treatment (PWHT) can partially restore toughness by relieving residual stresses and tempering brittle phases in the HAZ. Also, Innovative welding processes such as Friction Stir Welding (FSW) and low-hydrogen electrodes have been shown to improve low-temperature performance [8].

Despite the significant advancements in pipeline materials and welding technologies, ensuring the structural integrity of welded joints remains a major concern, particularly in High-Strength Low-Alloy (HSLA) steels used for oil and gas transportation. Studies have shown that the heat input and thermal cycles associated with welding processes can profoundly affect the microstructure and mechanical properties of the weldment, especially within the HAZ and the WM [9]. The Coarse-Grain Heat-Affected Zone (CGHAZ) and the intercortical CGHAZ are especially susceptible to microstructural transformations that can degrade toughness and overall performance [10]. While several investigations have addressed the influence of single-pass and automated welding techniques. [11]. In some literature, there is a lack of data, which shows concern regarding the impacts of multi-pass welding on different sub-regions of HSLA pipeline steels. These can rarely be accessed under varying thermal and mechanical conditions. This gap motivates the need for an in-depth analysis. In this study, the primary objective is to evaluate the effect of welding parameters on the microstructure changes and mechanical performance of the given material. This study also aims to observe the grain structure changes with the corresponding mechanical properties at different locations, namely, Weld Metal (WM), HAZ, and Base Metal (BM). The valuable insights into optimizing the welding practices for improved durability and performance of pipeline systems under operational conditions are accessed by varying welding parameters and analyzing their impact on sub-regions.

2. Materials and Experimental Procedure

In this study, we used API 5L X70 grade pipeline steel with a thickness of 20 mm. The plates were made using a thermo-mechanical control process and had a yield strength of 354.96 MPa, a tensile strength of 521.19 MPa, and an elongation at failure of 31.80%. The chemical composition of the base metal and welding wire was measured using an advanced ANACOM B2 optical emission spectrometer, and the results are shown in Table 1.

The experimental investigation employed API 5L X70 steel plates measuring 250 mm × 100 mm × 20 mm, which were carefully prepared for robotic MIG welding. Table 2 shows the Mechanical Properties of API 5L X70 steel material. Prior to welding, the plate edges were machined into a single V-groove configuration with a 30° included angle and 1.6 mm root face using a sequential process of shaping and precision milling with a T-max 80 carbide tool at 450 rpm (Figures 1(a) and 1(b)). A total of 9 identical specimen pairs were surface prepared through mechanical grinding to achieve uniform surface roughness ($Ra \leq 1.6$ μm) and remove contaminants. For joint assembly, the plates were tack-welded at both ends while maintaining a consistent 1.6 mm root gap using precision-ground spacers, with custom clamping fixtures employed to minimize distortion.

The welding is done with the welding machine system, which consists of a Yaskawa AR-1440 6-axis robotic arm with ±0.08 mm repeatability. It is also integrated with a constant voltage MIG power source, which is capable of 350 A maximum current. In this process, 1.2 mm diameter ER70S-6 copper-coated filler wire is used and passes through a four-roller push-pull system. This contains an 80% Argon + 20% CO_2 shielding gas mixture flowing at 15-20 L/min.

This welding was performed using a multi-pass technique in a controlled parameters environment. Initially, root pass is done for complete penetration, followed by filler and cap passes. During this pass, the temperature is maintained below 150°C, and a constant travel speed of 6 mm/sec. Quality assurance measures, which include pre-weld dimensional verification along with in-process monitoring of arc characteristics and post-weld examinations, were done. Macrographic sectioning and hardness testing, ensuring the production of consistent, high-quality weldments representative of industrial pipeline welding conditions, is also done after the welding process.

2.1. Design of Experiment

The experimental study employed the Taguchi method to systematically investigate the effects of three key welding parameters - voltage, current, and welding speed - each tested at three levels. An L9 orthogonal array was implemented to evaluate these parameters efficiently. The nine experimental runs were conducted while maintaining statistical validity. This approach shows an analysis of how the parameters affect and interactions on weld quality while minimizing resource requirements. The selected parameter ranges were based on preliminary trials and industry standards for robotic MIG welding of API 5L X70 steel during trial runs. The structured experimental design, as detailed in Table 3, facilitated reliable identification of optimal welding conditions for achieving desired weld properties with minimal defects. Table 4 shows process parameters and their values at different level. The specimen of welded pipeline steel was characterised for two primary mechanical tests, such as the tensile test and the

hardness test. All the specimens were prepared in accordance with standardized procedures and tested to ensure accuracy and repeatability. The Ultimate Tensile Strength (UTS), yield strength, and elongation of the welded joints were determined during the tensile test. The test specimens (Figure 6) were machined according to standard dimensions. This ensures that the gauge section is properly aligned with the weld region. A Universal Testing Machine (UTM) is used at room temperature. It specifically uses the UTN-40 model with a maximum load capacity of 400 kN. The test was conducted at a constant strain rate in compliance with ASTM E8/E8M standards. In the UTM machine, the load and elongation data were collected to generate stress-strain curves and evaluate mechanical behaviour.

2.2. Mechanical Testing

Vickers hardness testing was employed to assess the microhardness distribution across the weldment. The welded samples were sectioned transversely to the welding direction and parallel to the rolling direction to expose the cross-section. These sections were then subjected to a standard metallographic preparation process. This includes grinding and polishing with progressively finer abrasives. After that, final polishing is done using a 1 µm diamond paste to achieve a mirror-like finish suitable for hardness evaluation.

Hardness measurements were taken along the mid-thickness of the plate at the Traverse section across the weldment in the transverse direction. The evaluation covered the three primary zones of the weldment, such as BM, HAZ, and WM. The tests followed ASTM E384 guidelines to ensure the accuracy and reliability of the hardness profile. The weld configuration is shown in Figure 5. It shows the cross-sectional view of the weldments Specimens for different tests such as tensile, hardness, and microstructural analysis for this analysis the specimen were extracted from the transverse section of the weldments to ensure representative evaluation across the weld zones.

2.3. Characterization of the Welded Zone and Heat-Affected Zone

The microstructure of the base material used in this study, API 5L X70 pipeline steel, is characterized using an optical microscope. A sample is prepared with the standard, followed by metallographic techniques to ensure high-quality surface finishes for accurate analysis.

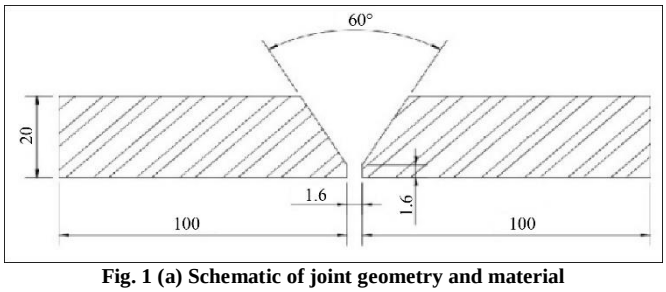

Fig. 1 (a) Schematic of joint geometry and material

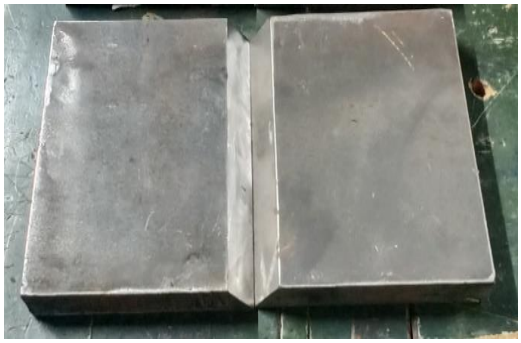

Fig. 1 (b) Actual groove for welding.

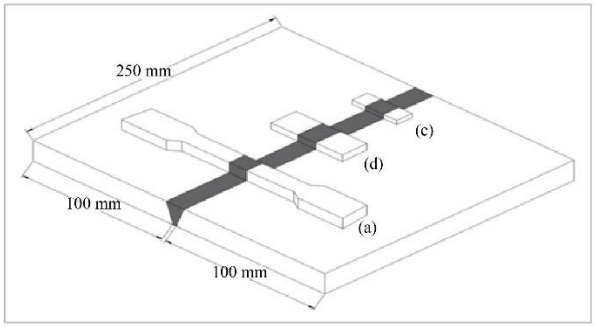

Fig. 2 The schematic illustration of the weld configuration

The specimens were first ground using silicon carbide abrasive papers with grit sizes ranging from 100 to 1200. This was followed by polishing with diamond paste, starting from 3 µm and finishing with 1 µm to achieve a mirror-like surface. Then the samples were etched with a 4% nital solution to reveal the grain boundaries and microstructural features. The prepared samples were examined under an optical microscope at various magnifications. The base metal displayed a predominantly ferritic matrix. The small amounts of pearlite distributed along the grain boundaries are also shown in the micrographs. These pearlite regions have contributed to the strength of the material. In some places, the ferrite matrix is also observed, which provides ductility and toughness. By the rolling process, the elongated grains are observed in the rolling direction. This elongated structure reflects the Thermo-Mechanical Controlled Processing (TMCP) applied during steel manufacturing. The observed microstructure serves as a baseline for evaluating changes induced by welding thermal cycles. It also provides insight into the inherent mechanical behavior of the base metal prior to welding. Understanding the base microstructure of given materials is essential for comparing it with the weld-affected zones. This characterization helps assess how welding parameters influence structural integrity and performance.

In this study, the ASTM E3-11 standards are referred to for the metallographic sample preparation. This sample preparation process includes processes such as sectioning, mounting, grinding, and polishing. The diamond paste is also used to obtain a mirror-like finish for microscopic analysis.

Optical microscopy was used to examine various regions such as the WM, HAZ, and base metal. The HAZ exhibited distinct microstructural changes compared to the base metal, which is due to the thermal cycle during welding. This affects the grain structure and phase distribution.

Table 1. Chemical composition of the API 5L X70 steel and filler wire in wt. %

Materials	Chemical composition in wt%							
	C	Mn	P	Si	S	Al	CE	Fe
Base metal	0.15	1.46	0.017	0.338	0.006	0.002	0.30	
Filler wire	0.15	1.85	0.025	1.15	--	--	--	--

Table 2. Mechanical properties of material

Property	API 5L X70	Electrode
Yield Strength (MPa)	354.96	451
Ultimate Tensile Strength (MPa)	521.19	537
Elongation (%)	31.80	24

Table 3. Welding speed for different welding current and voltage

Sr No.	Welding current (Amp)	Welding voltage (volts)	Welding speed (mm/sec)
1	140	24	2.7
2	140	26	3.2
3	140	28	3.6
4	160	24	3.2
5	160	26	3.6
6	160	28	2.7
7	180	24	3.6
8	180	26	2.7
9	180	28	3.2

Table 4. Process parameters and their values at different level

Sr. No	Parameter	Unit	Level1	Level 2	Level 3
1	Current	Amp	140	160	180
2	Voltage	Volts	24	26	28
3	Welding speed	mm/sec	2.7	3.15	3.6

3. Results and Discussion

3.1. Mechanical Properties Evaluation (Tensile Strength and Yield Strength)

The rectangular specimen was prepared to conduct the tensile test as per industry standards. This ensures the uniformity and comparability of results for each prepared specimen. Each specimen was subjected to a controlled uniaxial tensile load of 10 kg-f until fracture occurred. This process enabled the finding of key mechanical properties such as Ultimate Tensile Strength (UTS), yield strength, and elongation. During the test, the stress-strain behaviour of the material was also recorded. The observed behaviour provides the details of deformation characteristics and mechanical performance under tensile loading. After the test, fractured specimens are examined for the mode and origin of failure (Figures 3(a) and 3(b)).

Examination shows that most fractures initiated in the weld metal region. This confirms that it is the weakest part of the welded joint. This was consistent with the relatively lower tensile strength values observed for samples with weld metal failure compared to those fractured outside the weld zone. The standard stress-strain curves for these materials demonstrate the mechanical response of the specimens under load. The detailed statistical data, which includes average tensile strength values and variation across specimens, are given in Table 5. The fracture patterns and mechanical performance further support the conclusion that the weld metal's microstructural characteristics significantly influence the overall integrity and reliability of the welded joint.

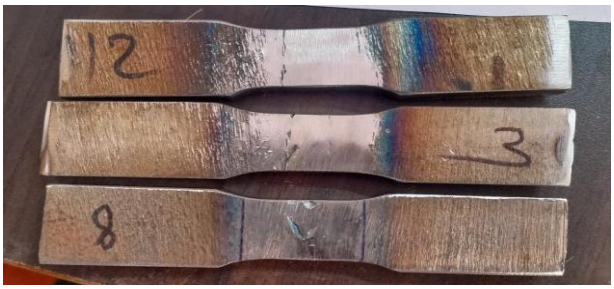

Fig. 3 (a) Specimen before tensile test

Fig. 3 (b) Failure zones of API 5L X70 steel welds after

3.2. Hardness Profile Across Weldments

Hardness test was carried out at three places, namely the Base Metal (BM), Weld Metal (WM), and Heat-Affected Zone (HAZ). The test results show that welding current is the most significant factor affecting hardness. An increase in hardness value was observed when the current increased from 140 A to 180 A. This rise in hardness values is mostly observed in the weld metal and HAZ regions. This increase in hardness with higher current can be attributed to increased heat input. This changes cooling rates and promotes the formation of harder microstructures such as bainite or martensite in the weld and HAZ. Welding voltage also shows its importance in the form of hardness. At higher voltage, the hardness value slightly increases. This is due to a wider arc and better fusion. Similarly, welding speed is also important for the hardness. Lower speeds resulted in greater heat input per unit length, which slightly increased hardness in localized regions. The HAZ typically showed higher hardness than the base metal, which confirms that microstructural transformation is significant due to thermal cycles. These findings show that welding parameters are important to control hardness distribution and maintain weld quality.

Table 5 shows the effect of welding parameters on the response. After the analysis, the main effects plot for SN ratios shows the influence of welding parameters on process stability (Figure 4(a)). From the analyses, welding current shows the most significant parameter in a positive effect. With increasing current from 140 A to 180 A, it consistently raises the SN ratio, which indicates improved robustness and performance. Voltage, on the other hand, has a relatively minor influence, with a slight increase in SN ratio as it moves from 24 V to 28 V. Welding speed displays a non-linear trend; the SN ratio peaks at 2.70 m/min, drops at 3.15 m/min, and then rises slightly at 3.60 m/min. Thus, the optimal levels for achieving higher SN ratios appear to be a current of 180 A, a voltage of 28 V, and a welding speed of 2.70 m/min.

In Figure 4(b), the main effects plot shows the significance values of current and welding speed. The mean response is highest at 180 A, again highlighting its strong positive effect. Voltage shows a peak at 26 V, followed by a drop at 28 V, suggesting an optimal level at 26 V. Welding speed has an inverse relationship with the mean response. As the speed increases, the mean decreases, with the highest response at the lowest speed (2.70 m/min). This shows that a higher current and lower welding speed are responsible for improving the mean output. The voltage has a moderate effect, with an optimal setting at 26 V. Both plots suggest fine-tuning the parameters can significantly enhance both the consistency and effectiveness of the robotic MIG welding process.

Table 5. Effect of welding parameters on the response

Sample No	Welding current	Welding voltage	Welding speed	Hardness in VH			Average Hardness in VH	Tensile Strength MPa	Heat Input KJ/mm
				BM	WM	HAZ			
1	140	24	2.7	176	145	160	161	467	1.2
2	140	26	3.2	190	160	167	173	442	1.07
3	140	28	3.6	160	181	144	162	442	1.09
4	160	24	3.2	158	173	145	159	439	1.3
5	160	26	3.6	161	172	150	161	445	1.8
6	160	28	2.7	165	184	153	168	448	2.6
7	180	24	3.6	167	176	166	170	444	2.6
8	180	26	2.7	160	188	194	190	478	2.9
9	180	28	3.2	168	183	155	169	452	2.0

Table 6. The hardness distribution across WM, HAZ, and BM

	Base metal			HAZ			Weld Metal		
Sample 1	148	150	151	168	170	169	181	180	182
Sample 2	150	155	153	160	165	166	179	181	175

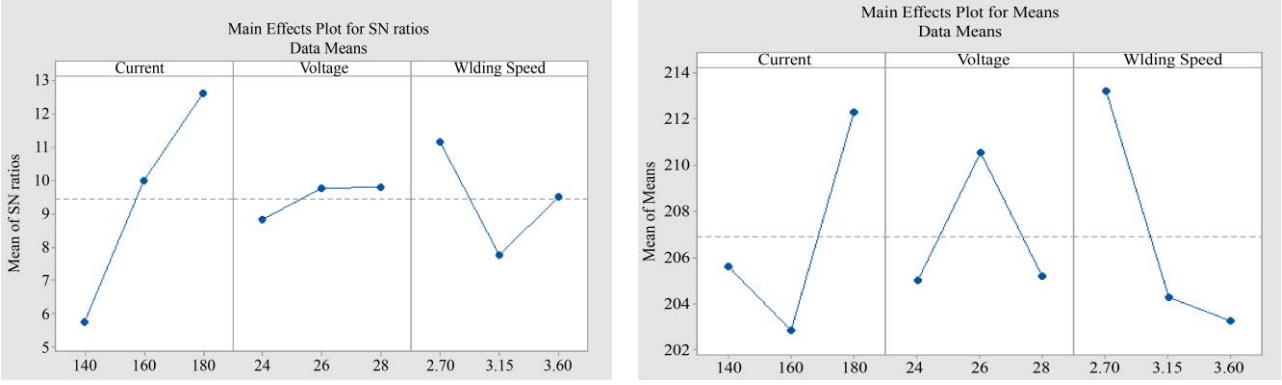

(a) **(b)**

Fig. 4 Mean effect plot for (a) SN ratio, and (b) Means.

Table 7. Charpy impact test results for the weld metals

Joint	Test Temperature	Charpy Fracture Energy (J)	Impact Toughness Requirement (J)
Robotic MIG welding	Room Temp (20^{0}°C)	Maximum:160 Minimum:146 Average:153	27
	- 40°C	Maximum:67 Minimum:45.5 Average:56.25	27
	- 60°C	Maximum:24 Minimum:9 Average:16.5	27
	- 80°C	Maximum:17 Minimum:9.5 Average:13.25	27
	- 100°C	Maximum:11 Minimum:4.5 Average:7.75	27

3.3. Impact Toughness at Room and Sub-Zero Temperatures

In the present study, the Charpy test evaluates the low-temperature impact toughness of welded joints in structural steel. The primary objective of this test is to determine the most effective welding method. These methods ensure high impact toughness in the HAZ and weld metal under cold service conditions. The material used was API 5L X70 pipeline steel, which was welded using robotic Metal Inert Gas (MIG) welding.

Tables 1 and 2 present the chemical composition and mechanical properties of the base metal. To accurately position the Charpy V-notch within the weld metal, and HAZ is prepared for accurate testing. The test specimens were prepared using a specific joint configuration. This setup enabled targeted assessment of the weld and HAZ toughness performance at sub-zero temperatures. This is essential for pipeline applications in cold environments. The hardness distribution across the weld cross-section, which includes WM, HAZ, and Base Metal (BM), is shown in Table 6. Based on the measurements, both the weld metal and the HAZ exhibit higher hardness values than the base material, indicating the absence of any softening zone within the welded joints. This suggests that the welding parameters used in the robotic MIG welding process were effective in maintaining or enhancing the mechanical integrity of the joint.

The elevated hardness values in the WM and HAZ are primarily attributed to refined microstructures and faster cooling rates during the welding process, which can lead to the formation of harder transformation products such as bainite or martensite. These findings confirm that the robotic MIG welding technique used in this study is suitable for producing structurally sound welds with favorable hardness characteristics for pipeline applications.

The Charpy impact test is a widely accepted method for experimentally determining the toughness of materials at various service temperatures in a simple and effective manner. In the present study, this test was applied to welded joints of API 5L X70 steel fabricated using robotic MIG welding, to assess their suitability for operation in low-temperature environments. The Charpy V-notch impact energy requirements, expressed in joules, are presented with respect

to the maximum nominal thickness and the minimum specified yield strength of carbon and low alloy steels, based on ASME (2004) guidelines. Since such specific toughness criteria are not provided in KS specifications, this ASME-based reference is crucial for establishing minimum performance requirements for steel used in cold climates. The data show that if the impact toughness of the welded joint exceeds the threshold value at a given temperature, the material can be considered safe and reliable for low-temperature applications. The absorbed energy values for the weld metal and heat-affected zones of the robotic MIG-welded joints were evaluated across a range of test temperatures, and the results are compiled in Tables 7 and 8. These tables also include the corresponding impact toughness requirements, allowing for a clear comparison of test results against standard benchmarks.

.

Table 8. Charpy impact test results for the HAZs

Joint	Test Temperature	Charpy Fracture Energy (J)	Impact Toughness Requirement (J)
Robotic MIG welding	Room Temp (20 ˚C)	Maximum:65 Minimum:33 Average:49	27
	- 40˚C	Maximum:35 Minimum:21 Average:28	27
	- 60˚C	Maximum:18 Minimum:9 Average:13.5	27
	- 80˚C	Maximum:14 Minimum:4.5 Average:9.25	27
	- 100˚C	Maximum:8.5 Minimum:6.5 Average:7.5	27

3.4. Microstructure Analysis

Nine MIG-welded joints were studied using Taguchi L9 designs, with microstructural characterization by SEM and optical microscopy for each sample. Micrographs were prepared for the BM, HAZ, and WZ. Below is a sample-wise breakdown, analytical guidelines for micrograph interpretation, and a summary.

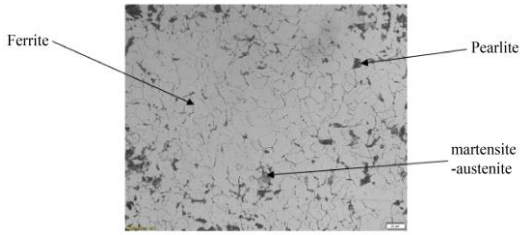

Fig. 5 The base metal

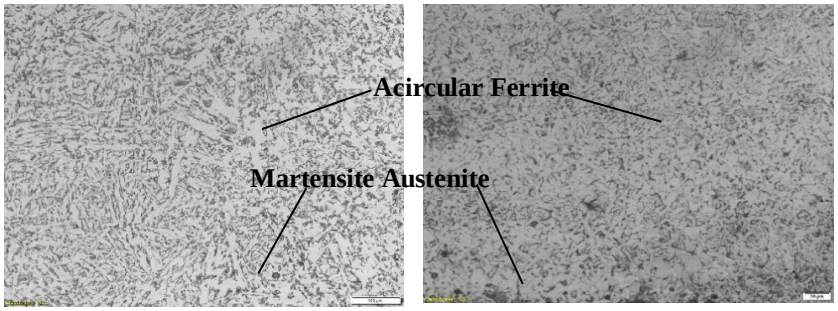

(a) **(b)**

Fig. 6 The microstructure of HAZ, (a) Lower heat input, and (b) Higher heat input.

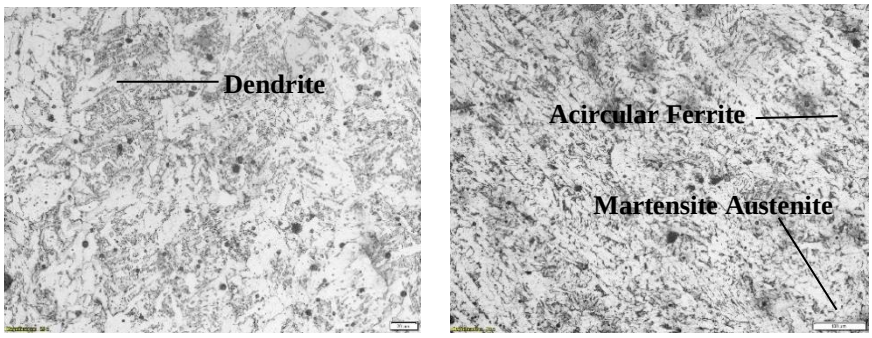

(a) **(b)**

Fig. 7 The microstructure of WZ, (a) Lower heat input, and (b) Higher heat input.

The base metal of API 5L X70 pipeline steel has a predominantly ferritic microstructure due to a direct consequence of Thermo-Mechanical Controlled Processing (TMCP), which is employed during steel manufacturing, elongated grains are aligned in the rolling direction. Optical microscope analysis shows a matrix consisting primarily of quasi-polygonal ferrite spread with acicular ferrite. Colonies of minor pearlite were distributed along grain boundaries. These Colonies contribute to the overall strength of the materials. These elongation grains were observed in the rolling direction, which is a characteristic feature of hot-rolled steels. These elongation grains reflect the thermo-mechanical history and plastic deformation during their manufacturing. Optical images with higher magnification show that small Martensite-Austenite (MA) constituents are marked as dark or blue-tinged regions (Figure 5). These MA are mainly located at grain triple junctions along with ferrite grain boundaries. The present microstructure shows the base metal with an optimal balance of mechanical properties. The ferritic matrix ensures excellent ductility and toughness, essential for pipeline applications subjected to complex loading conditions. The dispersed pearlite and MA constituents contribute to strength enhancement.

3.4.1. Heat-Affected Zone Microstructure

In HAZ, due to the heat during the welding, the microstructural changes are clearly shown in the material as compared with the base metal microstructure. Varying the heat input during welding, the different phase constituents and grain morphologies change systematically. The changes in HAZ include the formation of Widmanstätten ferrite. This is observed by its unique needle-like structure that is aligned like platelet structures. Due to rapid cooling, the Martensite-Austenite (MA) constituents increase rapidly during the welding thermal cycle. In the microstructure, the presence and morphology of acicular ferrite cause better toughness. It is seen with the development of the ferrite at higher heat input welds. It varies considerably depending on the higher temperature reached and the corresponding cooling rate. Both parameters are directly influenced by heat input parameters.

During the lower heat input conditions, finer grain structures were observed in the sample. In this microstructure, the proportion of bainite and pronounced acicular ferrite formation is higher (Figure 6(a)). It creates a microstructural configuration that is responsible for good strength. It also maintains adequate toughness and avoids excessive brittleness. The samples with higher heat input, particularly the sample, display significantly coarser grain structures with predominant Widmanstätten ferrite formation and elevated MA constituent content (Figure 6(b)). In these areas, martensite formation becomes increasingly evident when cooling rates exceed critical values for martensitic transformation. The HAZ consistently exhibits higher hardness values than both the base metal and the weld zone. It is confirmed by microhardness mapping and mechanical testing results.

3.4.2. Weld Zone Microstructure

The WZ microstructure shows the distinct characteristics that are changed after solidification processes. After solidification, it shows a considerably higher difference in microstructure than the base metal and heat-affected zone. These changes may be due to the heat treatment that involves melting, solidification, and multiple thermal cycles in multi-pass welding. The micrograph analysis shows that the WZ consists of a mixture of columnar and equiaxed ferrite grains. These columnar grains typically form near the fusion boundary. They grow epitaxially from partially melted base metal grains in the direction of maximum thermal gradient. The equiaxed grains develop in the weld center, where constitutional supercooling promotes nucleation-dominated growth. The phase constituents observed include various ferrite morphologies, pearlite colonies, bainitic regions, and discrete Martensite-Austenite (MA) islands, with their relative proportions. (Figure 7(a))

These distributions are strongly dependent on local cooling rates that vary spatially within the weld pool and temporally across different welding passes. Samples with lower heat input parameters exhibit more homogeneous ferritic microstructures, characterized by a relatively uniform grain size distribution and reduced residual stress concentrations. This contributes to balanced mechanical properties with adequate strength and ductility. Conversely, with a higher heat input, due to maximum current and voltage

settings, it exhibits a pronounced formation of hard martensitic and austenitic islands, along with clearly visible segregation lines and dendritic substructures (Figure 7(b)). The solidified microstructure, characterized by the Columnar-to-Equiaxed Transition (CET) and dendrite arm spacing, provides valuable insights into local cooling rates and thermal gradients. They have fine dendritic structures, which are generally associated with faster cooling and superior mechanical properties. However, coarser structures indicate slower cooling, potentially leading to reduced strength but improved ductility in certain cases.

4. Conclusion

This study shows that robotic MIG welding with optimized parameters produces high-quality API 5L X70 steel weldments suitable for critical pipeline applications. It shows that Welding current emerged as the most significant parameter affecting mechanical properties. The optimal conditions identified as 180 A current, 26 V voltage, and 2.7 mm/s speed, which yield a maximum tensile strength of 478 MPa and hardness of 190 HV at 2.9 kJ/mm heat input. Microstructural analysis shows that the HAZ has the most pronounced transformations. It shows the highest hardness due to the formation of Widmanstätten ferrite, bainite, and Martensite-Austenite (MA) constituents. Lower heat input conditions show finer grain structures with optimal strength-toughness balance. Higher heat inputs resulted in coarser grains with increased brittleness potential. Impact toughness testing confirmed that the welded joints maintain adequate toughness for cold-service applications down to -40°C. It meets ASME requirements for Arctic pipeline operations. In this study, the comprehensive microstructural characterization and mechanical property correlations established gives valuable guidance for industrial welding operations. It ensures the reliable performance and structural integrity of pipeline infrastructure systems in the oil and gas transmission sector. Future work should focus on post-weld heat treatment effects, extended low-temperature testing, and long-term service performance evaluation under actual operating conditions.

References

[1] V.Y. Antsev, N.A. Vitchuk, and V.V. Miroshnikov, "Improvement in Production Process for Pipelines Manufacturing Based on Quality Management Method," *Procedia Engineering*, vol. 206, pp. 950-957, 2017. [CrossRef] [Google Scholar] [Publisher Link]

[2] Hongwei Li et al., "Review of the State of the Art: Interactions between a Buried Pipeline and Frozen Soil," *Cold Regions Science and Technology*, vol. 157, pp. 171-186, 2019. [CrossRef] [Google Scholar] [Publisher Link]

[3] Mayur Pratap Singh et al., "The Structural Integrity of High-Strength Welded Pipeline Steels: A Review," *International Journal of Structural Integrity*, vol. 12, no. 3, pp. 470-496, 2021. [CrossRef] [Google Scholar] [Publisher Link]

[4] Saadat Ali Rizvi, and Wajahat Ali, "Microstructure Behaviour Evolutions in the Heat-Affected Zone and Fusion Zones of the AISI 304 Stainless Steel Weldment in Double Pass Weld," *Advances in Manufacturing Engineering*, pp. 179-187, 2024. [CrossRef] [Google Scholar] [Publisher Link]

[5] Jagesvar Verma, and Ravindra Vasantrao Taiwade, "Effect of Welding Processes and Conditions on the Microstructure, Mechanical Properties and Corrosion Resistance of Duplex Stainless Steel Weldments-A Review," *Journal of Manufacturing Processes*, vol. 25, pp. 134-152, 2017. [CrossRef] [Google Scholar] [Publisher Link]

[6] A. Lambert-Perlade et al., "Mechanisms and Modeling of Cleavage Fracture in Simulated Heat-Affected Zone Microstructures of a High-Strength Low Alloy Steel," *Metallurgical and Materials Transactions A*, vol. 35, no. 13, pp. 1039-1053, 2004. [CrossRef] [Google Scholar] [Publisher Link]

[7] Huiming Ding et al., "Tensile Properties and Impact Toughness of S30408 Stainless Steel and its Welded Joints at Cryogenic Temperatures," *Cryogenics*, vol. 92, pp. 50-59, 2018. [CrossRef] [Google Scholar] [Publisher Link]

[8] Junyeong Kim et al., "Continuous Tempering Effect Induced PWHT Alternative Technology Using Wire arc Additive Manufacturing for Application in Replacing Nuclear Pressurized Water Reactor System Repairing: CALPHAD, FEM Simulation, and EBSD Investigation," *Journal of Materials Research and Technology*, vol. 25, pp. 2961-2988, 2023. [CrossRef] [Google Scholar] [Publisher Link]

[9] Guangming Xie et al., "Microstructure and Toughness of Thick-Gauge Pipeline Steel Joint Via Double-Sided Friction Stir Welding Combined with Preheating," *International Journal of Minerals, Metallurgy and Materials*, vol. 30, no. 4, pp. 724-733, 2023. [CrossRef] [Google Scholar] [Publisher Link]

[10] Shou Liu et al., "Comparison of Fracture Toughness in the Coarse-Grain Heat-Affected Zone of X80 Pipelines Girth-Welded under Conventional and Ultra-Low Heat Input," *Materials*, vol. 15, no. 21, pp. 1-12, 2022. [CrossRef] [Google Scholar] [Publisher Link]

[11] Wei Li et al., "Microstructure Evolution and Impact Toughness Variation for High Strength Steel Multi-Pass Weld Metals with Various Cooling Rates," *Journal of Manufacturing Processes*, vol. 65, pp. 245-257, 2021. [CrossRef] [Google Scholar] [Publisher Link]